ChemComm

COMMUNICATION

View Article Online
View Journal | View Issue

Cite this: *Chem. Commun.*, 2024, **60**, 5614

Received 30th January 2024,
Accepted 25th April 2024

DOI: 10.1039/d4cc00463a

rsc.li/chemcomm

Borophene: a piezocatalyst for water remediation†

Aditi Sharma,[ab] Upasana Bhardwaj,[a] Maya Marinova,[c] Antonio Da Costa,[d] Anthony Ferri,[d] Sébastien Royer,[b] Himmat Singh Kushwaha *[ae] and Jérémy Dhainaut *[b]

Borophene is an emerging two-dimensional material exhibiting exceptional piezocatalytic activity under the influence of ultrasonic vibrations, as exemplified herein by the decomposition of highly stable organic dyes in water. After 6 minutes of exposure, borophene sheets converted up to 92 percent of a mixture of dye molecules at room temperature.

Piezocatalysis is an emerging technique based on the piezoelectric effect of materials lacking a center of symmetry. Such materials deform themselves under the effect of mechanical vibrations, causing spontaneous polarization. Then, the free charge carriers inside the materials are separated through the induced piezopotential and can migrate to the surface to further engage in redox reactions.[1] The piezoelectricity produced by mechanical distortion in such materials has found widespread application in sensing, actuators, and high-voltage generators.[2]

Most known piezoelectric devices are composed of bulk materials like ceramics and single crystals. The application of nanosized piezoelectric materials is newer.[1] In particular, two-dimensional materials have garnered a great deal of interest due to their high surface-to-volume ratio and exceptional electronic properties, which grant them with a greater potential for various applications such as energy storage, sensing, electronics, and aerospace structures than their bulk form.[2] In 2014, it was discovered for the first time that MoS_2 nanosheets exhibit substantial piezoelectric properties.[3] After the development of 2D materials such as graphene,[4] silicene,[5] hexagonal boron nitride,[6] stanine, aluminum nitride sheet, phosphorene,[7] arsenene, molybdenum disulfide, and antimonene, 2D boron sheets known as borophene were unveiled.[8] Borophene has rich architectural diversity, exhibiting unique physical and chemical properties including ultrahigh thermal conductance, superconductivity, high carrier mobility, presence of Dirac fermions, and optical transparency.[9] Boron-related 2D compounds are distinguished from other 2D materials by their polymorphism,[10] *i.e.*, the capacity of boron to create multicenter bonding arrangements enabling the formation of a large variety of stable 2D phases. In particular, the β_{12} phase of borophene is anisotropic. Due to this, the unique character of boron–boron multicenter bonds has been elucidated theoretically, resulting in great bending flexibility and optimum strength along various orientations of the borophene. As a result, the findings suggest that borophene is a promising material, with potential applications as a piezocatalyst, among others.[11]

Initially, borophene was synthesized by chemical vapor deposition on a metal substrate.[12] However, this method produces limited amounts of borophene. For larger synthesis scales, a modified Hummers' method has been recently proposed.[11] The resulting two-dimensional material is easily deformable, and its flat surface gives a large area for capturing mechanical energy. Under ultrasonication, these nanosheets readily degrade organic pollutants, for instance organic dyes in water. By monitoring the reactive radicals produced during the piezocatalytic process, a degradation mechanism of organic dyes involving superoxide ($^{\bullet}O_2^-$) and hydroxyl ($^{\bullet}OH$) oxidant radicals is proposed.

The XRD pattern of the synthesized borophene sheets is depicted in Fig. S1a (ESI†), and it matches well with the β-rhombohedral crystalline structure of boron (ICDD card no. 00-031-0207).[13] The reduced peaks intensity may suggest that upon formation, the crystals grow following a preferential orientation.[14] Hence, to confirm the formation of borophene sheets, their Raman spectrum is depicted in Fig. S1b (ESI†).

[a] *Materials Research Centre, Malaviya National Institute of Technology Jaipur (MNITJ), India*
[b] *Univ. Lille, CNRS, Centrale Lille, Univ. Artois, UMR 8181 – UCCS – Unité de Catalyse et Chimie du Solide, Lille F-59000, France. E-mail: jeremy.dhainaut@univ-lille.fr*
[c] *Université de Lille, CNRS, INRA, Centrale Lille, Université Artois, FR 2638 – IMEC – Institut Michel-Eugène Chevreul, Lille 59000, France*
[d] *Univ. Artois, CNRS, Centrale Lille, Univ. Lille, UMR 8181, Unité de Catalyse et Chimie du Solide (UCCS), Lens F-62300, France*
[e] *Shodh Lab, Suresh Gyan Vihar University Jaipur, 302017, India. E-mail: himmat1.singh@mygyanvihar.com*

† Electronic supplementary information (ESI) available: Experimental protocols, additional characterization (XRD, Raman, XPS, AFM), oscilloscope measurements, additional catalytic data and scavenging experiments. See DOI: https://doi.org/10.1039/d4cc00463a

The improved Hummer's process produced borophene sheets with distinct Raman peaks, which matches well with the boron appearing at 234 cm^{-1}, 379.15 cm^{-1}, 696 cm^{-1}, 911.05 cm^{-1}, 1062 cm^{-1} and 1155 cm^{-1}.[15] Borophene, unlike graphene, is anisotropic; as a result, its symmetry axes are not identical, resulting in multiple distinctive peaks.[11] High resolution XPS, as shown in Fig. S1c (ESI†), was further applied to evaluate the surface composition of borophene. The as synthesized borophene displays three peaks in the B 1s spectrum centered at 192.5, 189.1, and 187.7 eV, showing that B created three types of bonding structures. The principal component related to a B–B bond at 187.7 eV is comparable with the previously reported values for bulk B (187.3–187.9 eV),[16] while the peak attributed to the B–O bond in a boron-rich oxide is located at 189.1 eV. The 192.5 eV signal appears to be related to the production of B_2O_3, indicating that borophene may be partially oxidized due to its large contact area.[17]

Representative BF-TEM and HR-TEM images together with the respective SAED pattern and fast Fourier transform (FFT) pattern, respectively, are presented in Fig. 1a and b and their insets. These images were taken on the powder sample. A representative HAADF image in the cross-section is shown in Fig. S2 (ESI†). The SAED pattern has been indexed and best matches with the [100] zone axis of the β-rhombohedral boron structure (space group: $R\bar{3}m$ (166) and a = 10.9251(2) Å; b = 10.9251(2) Å; c = 23.8143(8) Å).[18] The thickness of the borophene sheets varies between approximately 5 nm and 15 nm, as shown in Fig. S3 (ESI†). These sheets have parallel atomic ridges and are crystalline. The interplanar distance measured (0.326 nm) from the cross-sectional HAADF image matches with the (300) plane of β_{12} borophene, which agrees with the TEM images.[19] Fig. S3 (ESI†) shows atomic force microscopy (AFM) images depicting that the thickness of the borophene stacked nanosheets ranges from 2 to 15 nm, matching with TEM observations. Of note, the lateral dimensions of the as-produced borophene can also be observed and are above 200 nm.

A PFM approach was used to probe the piezoelectric properties of borophene nanosheets at the nanoscale. When an AC driving voltage is applied to the sample *via* the AFM tip, the ensuing mechanical deformation of the material is induced due to the converse piezoelectric effect.[20] The as-grown out-of-plane (OP) and in-plane (IP) amplitude piezoresponse patterns measured over the surface of the borophene sample are presented in Fig. 2b and c, respectively, simultaneously recorded with the topography in Fig. 2a. As a remark, the poor quality of the AFM topographic image presented in Fig. 2a is mainly due to the contact mode required for simultaneously recording the topographic and piezoresponse signals. Nonetheless, a strong piezoelectric response is detected along both the OP and IP direction, as revealed by the bright contrasts. By superimposing a continuous DC bias voltage (voltage pulse bias ramps from −10 V to +10 V) on the intermittent AC signal, amplitude piezoresponse loops can be recorded. As seen in Fig. 2d, a well-defined butterfly-shaped loop is obtained, evidencing clear piezoelectric behavior in borophene,[21] in agreement with the amplitude PFM pattern in Fig. 2b.

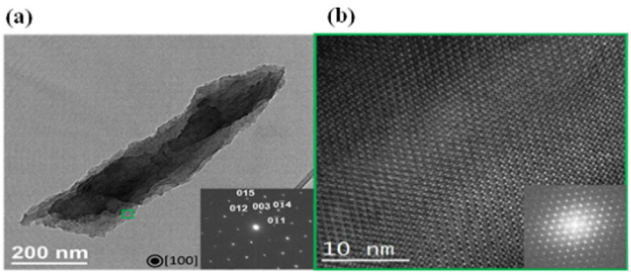

Fig. 1 (a) and (b) BF-TEM and HR-TEM images with the SAED and fast Fourier transform (FFT) patterns, respectively.

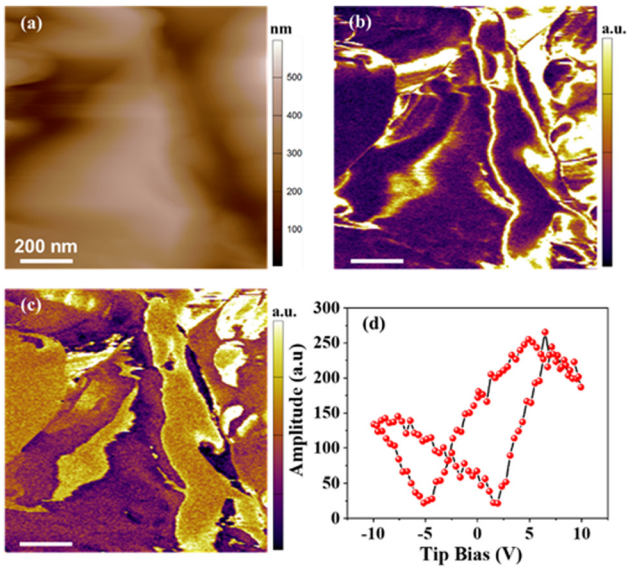

Fig. 2 (a) AFM morphology, (b) amplitude OP-PFM, and (c) amplitude IP-PFM images simultaneously recorded on the borophene surface, and (d) characteristic amplitude piezoresponse loop recorded on borophene nanosheets.

Fig. S4a (ESI†) shows digital scanning oscilloscope (DSO) measurements of the open circuit voltage response of mechanically stressed borophene sheets. Under bending conditions, the maximum voltage reaches up to 0.078 V, and it reaches 0.18 V when pressure is exerted by manual tapping. When pressure is imposed onto the borophene sheets, the induced piezopotential generates positive impulses, and when pressure is removed from the borophene sheets, the induced piezopotential generates negative impulses. The piezoelectric effect was not observed in the absence of vibrations, implying that no pressure was applied to or removed from the borophene sheets.[22] Fig. S4b (ESI†) shows the piezo current response for the borophene sheets. It has good charge separation efficiency and high electron mobility.

Borophene was applied to the degradation of organic pollutants, and the piezocatalytic results are depicted in Fig. 3a and b. In the case of methylene blue (MB), the absorbance peak at 668 nm decreases significantly from 6 minutes of ultrasonic vibrations (Fig. S5a, ESI†). Fig. S5b (ESI†) shows the

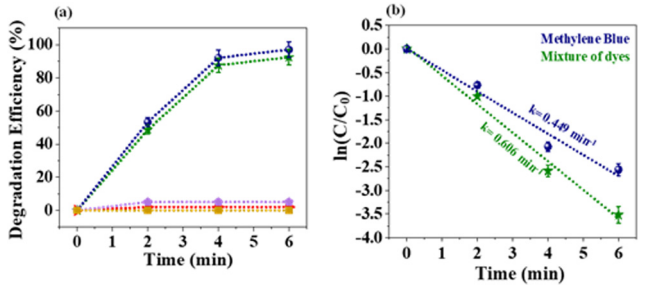

Fig. 3 (a) Degradation efficiency of borophene (blue: methylene blue + borophene + ultrasounds, green: mixture of dyes + borophene + ultrasounds, purple: methylene blue + borophene, red: mixture of dyes + borophene, orange: methylene blue + ultrasounds), and (b) kinetic order curves.

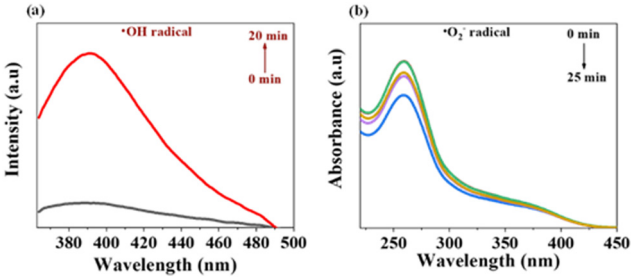

Fig. 4 (a) Photoluminescence spectra for the detection of OH• radicals by using terephthalic acid, and (b) degradation of nitroblue tetrazolium (NBT) under the piezocatalytic effect to confirm the production of super oxide radicals ($^{\bullet}O_2^-$).

degradation of a mixture of dyes (rhodamine B, MB, methyl orange, and rose Bengal) following 6 minutes of exposure time under ultrasonic vibrations. It has been shown that 92% of all dye molecules were readily deteriorated at room temperature and without the addition of an oxidant as typically done in photocatalysis (H_2O_2, persulfates).[23] The relating decomposition ratios are summed up in Fig. S5c (ESI†). MB and a mixture of dyes were degraded up to 97% and 92% after 6 minutes, respectively. Fig. 3a depicts the degradation efficiency curve, which was computed by subtracting the starting concentration from the concentration obtained after treatment. Importantly, no degradation occurs when only ultrasonic vibrations or borophene are applied to organic dyes. The corresponding degradation rate constants were determined by fitting the empirical observations to the pseudo-first order kinetic rate equation ($-\ln kt = C/C_0$), as shown in Fig. 3b. Under ultrasonication, the degradation rate constant of MB is $k = -0.4495\ \text{min}^{-1}$, whereas the rate constant for the mixture of dyes is $k = -0.60675\ \text{min}^{-1}$. In addition, the recyclability of borophene for degrading MB was examined without pre-treatment. The degradation efficiency was slightly reduced from the sixth cycle (−3% compared to the initial rate), confirming the robustness of borophene as a piezocatalyst for long-term applications (Fig. S6a, ESI†). The structural stability of borophene nanosheets also provides solid proof that the degradation of MB is caused by the piezocatalytic effect of borophene, rather than by any direct chemical reaction between borophene and the organic dye. However, as shown in Fig. S6b and c (ESI†), very little boron oxide (B_2O_3) is formed after six cycles (36 minutes total exposure time). Table S1 (ESI†) finally compares different piezocatalytic systems applied to MB degradation, highlighting the superior performances of borophene.

The scavenger study was carried out to investigate the involvement of active radical species in the breakdown of MB by borophene sheets *via* a piezocatalytic mechanism. Isopropyl alcohol (IPA) scavenges hydroxy radicals (OH•), para-benzoquinone (BQ) scavenges superoxide ($^{\bullet}O_2^-$), and ethylenediaminetetraacetate (EDTA) scavenges holes (h^+). These scavengers were coupled with borophene sheets and the MB solution. As demonstrated in Fig. S7 (ESI†), the breakdown efficiency of MB molecules was dramatically reduced when isopropanol alcohol (IPA) and benzoquinone (BQ) were added to the MB aqueous solution. However, when disodium ethylenediaminetetraacetate (EDTA-2Na) was added to the reaction solution, only a minor decrease in degradation was detected. The findings indicate that the $^{\bullet}OH$ and $^{\bullet}O_2^-$ radicals were generated and served as the primary reactive species in the piezocatalytic process.[24] Throughout the piezocatalytic process, fluorescence spectroscopy was employed to detect the formation of hydroxyl radicals ($^{\bullet}OH$) as they rapidly interact with terephthalic acid to form 2-hydroxyterephthalic acid, a highly fluorescent drug with a signal at 425 nm under 315 nm excitation.[25] As observed in Fig. 4a, under ultrasonic irradiation, borophene produces a consequent amount of hydroxyl radicals, which are one of the main active species in liquid-phase advanced oxidation processes. Furthermore, the degradation of nitro blue tetrazolium chloride, which is a scavenger for super oxide radicals ($^{\bullet}O_2^-$), was carried out under the same conditions as dye degradation.[8] As illustrated in Fig. 4b, its degradation shows the consequent formation of $^{\bullet}O_2^-$.

Based on the above findings, a potential piezocatalytic mechanism interpretation is proposed in Fig. S9 (ESI†). Initially, bound charges on the piezoelectric material's surface are in equilibrium with screening charges, resulting in an electrically neutral material.[26] Due to compressive stress caused by the piezoelectric action, the amplitude of polarization will be lowered. This, in turn, can cause charge carrier redistribution and the release of extra screening charges from the surface. As a result, the surplus charges disperse into the solution and become free charges, combining with water molecules to generate reactive species like $^{\bullet}OH$ and $^{\bullet}O_2^-$.[27] When mechanical stress is imposed at its maximum level, the polarized charges will be minimized. The additional screening charges will continue to be released until the material attains a new electrostatic balance.[28] When the applied stress is released, then the newly formed electrostatic equilibria will break again, increasing the polarization. The charges will thus be adsorbed from the surroundings to balance the bound charges caused by the piezoelectric effect. In a similar manner to forward loading, the redox reactions at the solid–liquid interface will not last long due to the depletion of the surface charge. The free charges (e^- and h^+) that were spent by redox reactions can be produced again thermally by the mechanical energy (ultrasonic vibrations), producing an apparent piezocatalytic effect. The

main reactions that occur in the degradation mechanism are depicted in eqn (1)–(4):

$$\text{Borophene} + \text{US vibrations} \rightarrow \text{borophene}\ (e^- + h^+) \quad (1)$$

$$O_2 + e^- \rightarrow {}^{\bullet}O_2^- \quad (2)$$

$$H_2O + h^+ \rightarrow {}^{\bullet}OH \quad (3)$$

$${}^{\bullet}O_2^-/{}^{\bullet}OH + \text{pollutants} \rightarrow \text{degraded products} \quad (4)$$

In conclusion, this paper describes the synthesis of borophene nanosheets, as well as their characterization. In particular, the formation of a piezo-potential within the borophene nanosheets under mechanical stress was measured to be ~0.2 V. Utilizing ultrasonic vibration energy, the piezocatalytic ability of borophene nanosheets to decompose single and mixtures of organic dyes has been investigated. Under these conditions, borophene nanosheets efficiently degrade all types of dye molecules. Hydroxyl ($^{\bullet}OH$) and superoxide ($^{\bullet}O_2^-$) radicals are the primary oxidizing species that are produced from polarized electric charges. Our work will encourage additional research in the fields of piezocatalysis over borophene-based materials, especially in the field of water remediation.

H. S. K., J. D. and S. R. conceived and designed the project. A. S. prepared the borophene, conducted most characterization, and did all catalytic tests. U. B. measured the piezo potential and piezo current response with DSO. M. M. conducted HR-TEM observations, and analysed and discussed HR-TEM data. A. D. C. conducted PFM measurements. A. F. analysed and discussed the PFM data. A. S., J. D., H. S. K., and S. R. analysed all other data. A. S. wrote the original manuscript. All authors discussed the results and commented on the manuscript.

A. S. is grateful to Campus France for the Eiffel Excellence Scholarship. The CNRS, the Chevreul Institute (FR 2638), the Ministère de l'Enseignement Supérieur et de la Recherche, the Région Hauts-de-France and the ERDF are acknowledged for supporting this work.

Conflicts of interest

There are no conflicts to declare.

Notes and references

1 J. Li, S. Chen, W. Liu, R. Fu, S. Tu, Y. Zhao, L. Dong, B. Yan and Y. Gu, *J. Phys. Chem. C*, 2019, **123**, 11378.
2 H. Cui, X. Zhang and D. Chen, *Appl. Phys. A: Mater. Sci. Process.*, 2018, **124**, 636.
3 W. Wu, L. Wang, Y. Li, F. Zhang, L. Lin, S. Niu, D. Chenet, X. Zhang, Y. Hao, T. F. Heinz, J. Hone and Z. L. Wang, *Nature*, 2014, **514**, 470.
4 A. A. Balandin, *Nat. Mater.*, 2011, **10**, 569.
5 H. Dai, P. Xiao and Q. Lou, *Phys. Status Solidi A*, 2011, **208**, 1714.
6 J. Dauber, A. A. Sagade, M. Oellers, K. Watanabe, T. Taniguchi, D. Neumaier and C. Stampfer, *Appl. Phys. Lett.*, 2015, **106**, 193501.
7 S. Zhang, S. Guo, Z. Chen, Y. Wang, H. Gao, J. Gómez-Herrero, P. Ares, F. Zamora, Z. Zhu and H. Zeng, *Chem. Soc. Rev.*, 2018, **47**, 982.
8 Z. A. Piazza, H. S. Hu, W. L. Li, Y. F. Zhao, J. Li and L. S. Wang, *Nat. Commun.*, 2014, **5**, 3113.
9 S. Y. Xie, Y. Wang and X. Bin Li, *Adv. Mater.*, 2019, **31**, 1900392; A. J. Mannix, X. F. Zhou, B. Kiraly, J. D. Wood, D. Alducin, B. D. Myers, X. Liu, B. L. Fisher, U. Santiago, J. R. Guest, M. J. Yacaman, A. Ponce, A. R. Oganov, M. C. Hersam and N. P. Guisinger, *Science*, 2015, **350**, 1513; B. Feng, J. Zhang, Q. Zhong, W. Li, S. Li, H. Li, P. Cheng, S. Meng, L. Chen and K. Wu, *Nat. Chem.*, 2016, **8**, 563; A. J. Mannix, Z. Zhang, N. P. Guisinger, B. I. Yakobson and M. C. Hersam, *Nat. Nanotechnol.*, 2018, **13**, 444.
10 Y. Jiao, F. Ma, J. Bell, A. Bilic and A. Du, *Angew. Chem., Int. Ed.*, 2016, **55**, 10292; T. Kondo, *Sci. Technol. Adv. Mater.*, 2017, **18**, 780; Z. Zhang, E. S. Penev and B. I. Yakobson, *Chem. Soc. Rev.*, 2017, **46**, 6746.
11 C. Hou, G. Tai, Y. Liu and X. Liu, *Nano Res.*, 2022, **15**, 2537; Z. Zhang, E. S. Penev and B. I. Yakobson, *Chem. Soc. Rev.*, 2017, **46**, 6746; P. Ranjan, T. K. Sahu, R. Bhushan, S. S. R. K. C. Yamijala, D. J. Late, P. Kumar and A. Vinu, *Adv. Mater.*, 2019, **31**, 1900353; P. Ranjan, J. M. Lee, P. Kumar and A. Vinu, *Adv. Mater.*, 2020, **32**, 2000531.
12 M. Ou, X. Wang, L. Yu, C. Liu, W. Tao, X. Ji and L. Mei, *Adv. Sci.*, 2021, **8**, 2001801; Y. Liu, G. Tai, C. Hou, Z. Wu and X. Liang, *ACS Appl. Mater. Interfaces*, 2023, **15**, 14566.
13 N. Taşaltın, S. Güllülü and S. Karakuş, *Inorg. Chem. Commun.*, 2022, **136**, 109150.
14 F. Zhang, L. She, C. Jia, X. He, Q. Li, J. Sun, Z. Lei and Z. H. Liu, *RSC Adv.*, 2020, **10**, 27532.
15 Q. Fan, C. Choi, C. Yan, Y. Liu, J. Qiu, S. Hong, Y. Jung and Z. Sun, *Chem. Commun.*, 2019, **55**, 4246.
16 T. T. Xu, J. G. Zheng, N. Wu, A. W. Nicholls, J. R. Roth, D. A. Dikin and R. S. Ruoff, *Nano Lett.*, 2004, **4**, 963.
17 H. Li, L. Jing, W. Liu, J. Lin, R. Y. Tay, S. H. Tsang and E. H. T. Teo, *ACS Nano*, 2018, **12**, 1262.
18 B. Callmer, *Acta Crystallogr., Sect. B*, 1977, **33**, 1951.
19 D. Ma, R. Wang, J. Zhao, Q. Chen, L. Wu, D. Li, L. Su, X. Jiang, Z. Luo, Y. Ge, J. Li, Y. Zhang and H. Zhang, *Nanoscale*, 2020, **12**, 5313; C. Taşaltın, T. A. Türkmen, N. Taşaltın and S. Karakuş, *J. Mater. Sci.: Mater. Electron.*, 2021, **32**, 10750.
20 A. Gruverman, M. Alexe and D. Meier, *Nat. Commun.*, 2019, **10**, 1661.
21 Q. Tang, J. Wu, D. Kim, C. Franco, A. Terzopoulou, A. Veciana, J. Puigmartí-Luis, X. Z. Chen, B. J. Nelson and S. Pané, *Adv. Funct. Mater.*, 2022, **32**, 2202180; E. Lin, N. Qin, J. Wu, B. Yuan, Z. Kang and D. Bao, *ACS Appl. Mater. Interfaces*, 2020, **12**, 14005.
22 A. Sharma, U. Bhardwaj and H. S. Kushwaha, *Mater. Adv.*, 2021, **2**, 2649; A. Sharma, U. Bhardwaj, D. Jain and H. S. Kushwaha, *ACS Omega*, 2022, **7**, 7595.
23 D. Ma, H. Yi, C. Lai, X. Liu, X. Huo, Z. An, L. Li, Y. Fu, B. Li, M. Zhang, L. Qin, S. Liu and L. Yang, *Chemosphere*, 2021, **275**, 130104.
24 F. Bößl, T. P. Comyn, P. I. Cowin, F. R. García-García and I. Tudela, *Chem. Eng. J. Adv.*, 2021, **7**, 100133.
25 A. Sharma, U. Bhardwaj and H. S. Kushwaha, *Catal. Sci. Technol.*, 2022, **12**, 812.
26 O. Copie, N. Chevalier, G. Le Rhun, C. L. Rountree, D. Martinotti, S. Gonzalez, C. Mathieu, O. Renault and N. Barrett, *ACS Appl. Mater. Interfaces*, 2017, **9**, 29311.
27 J. Wu, W. Mao, Z. Wu, X. Xu, H. You, A. Xue and Y. Jia, *Nanoscale*, 2016, **8**, 7343–7350; H. Lei, M. Wu, Y. Liu, F. Mo, J. Chen, S. Ji, Y. Zou and X. Dong, *Chin. Chem. Lett.*, 2021, **32**, 2317.
28 Y. Zi, L. Lin, J. Wang, S. Wang, J. Chen, X. Fan, P. K. Yang, F. Yi and Z. L. Wang, *Adv. Mater.*, 2015, **27**, 2340.